J Physiol 593.3 (2015) pp 619–634

The Journal of Physiology

Electrophysiological properties of laryngeal motoneurones in rats submitted to chronic intermittent hypoxia

Davi J. A. Moraes and Benedito H. Machado

Department of Physiology, School of Medicine of Ribeirão Preto, University of São Paulo, Ribeirão Preto, SP, Brazil

Key points

- The respiratory control of the glottis by laryngeal motoneurones is characterized by inspiratory abduction and post-inspiratory adduction causing decreases and increases in upper airway resistance, respectively.
- Chronic intermittent hypoxia (CIH), an important component of obstructive sleep apnoea, exaggerated glottal abduction (before inspiration), associated with active expiration and decreased glottal adduction during post-inspiration.
- CIH increased the inspiratory and decreased the post-inspiratory laryngeal motoneurone activities, which is not associated to changes in their intrinsic electrophysiological properties.
- We conclude that the changes in the respiratory network after CIH seem to be an adaptive process required for an appropriated pulmonary ventilation and control of upper airway resistance under intermittent episodes of hypoxia.

Abstract To keep an appropriate airflow to and from the lungs under physiological conditions a precise neural co-ordination of the upper airway resistance by laryngeal motoneurones in the nucleus ambiguus is essential. Chronic intermittent hypoxia (CIH), an important component of obstructive sleep apnoea, may alter these fine mechanisms. Here, using nerve and whole cell patch clamp recordings in *in situ* preparations of rats we investigated the effects of CIH on the respiratory control of the upper airway resistance, on the electrophysiological properties of laryngeal motoneurones in the nucleus ambiguus, and the role of carotid body (CB) afferents to the brainstem on the underlying mechanisms of these effects. CIH rats exhibited longer pre-inspiratory and lower post-inspiratory superior laryngeal nerve activities than control rats. These changes produced exaggerated glottal abduction (before inspiration) and decreased glottal adduction during post-inspiration, indicating a reduction of upper airway resistance during these respiratory phases after CIH. CB denervation abolished these changes produced by CIH. Regarding choline acetyltransferase positive-laryngeal motoneurones, CIH increased the firing frequency of inspiratory and decreased the firing frequency of post-inspiratory laryngeal motoneurones, without changes in their intrinsic electrophysiological properties. These data show that the effects of CIH on the upper airway resistance and laryngeal motoneurones activities are driven by the integrity of CB, which afferents induce changes in the central respiratory generators in the brainstem. These neural changes in the respiratory network seem to be an adaptive process required for an appropriated pulmonary ventilation and control of upper airway resistance under intermittent episodes of hypoxia.

DOI: 10.1113/jphysiol.2014.283085

(Resubmitted 24 August 2014; accepted after revision 17 November 2014; first published online 21 November 2014)
Corresponding author: Davi J. A. Moraes, Ph.D. Department of Physiology, School of Medicine of Ribeirão Preto, University of São Paulo, 14049–900, Ribeirão Preto, SP, Brazil. Email: davimoraes@rfi.fmrp.usp.br

Abbreviations AbN, abdominal nerve; ADN, aortic depressor nerve; AHP, afterhyperpolarization potential; AP, action potential; BötC, Bötzinger Complex; CB, carotid body; CBD, carotid body denervation; Chat, choline acetyltransferase; CIH, chronic intermittent hypoxia; E2, second half of expiration; F_{I,O_2}, fraction of inspired oxygen; I_A, outward transient K^+ current; I_h, hyperpolarization-activated inward current; LVA, low voltage activated Ca^{2+} currents; NA, nucleus ambiguus; OSA, obstructive sleep apnoea; PN, phrenic nerve; pre-BötC, pre-Bötzinger Complex; RLN, recurrent laryngeal nerve; RMP, resting membrane potential; SGP, subglottal pressure; SLN, superior laryngeal nerve; tSN, thoracic sympathetic nerve; TTX, tetrodotoxin.

Introduction

The laryngeal muscles control upper airway resistance for multiple functions, including breathing (Shiba *et al.* 2007; Fregosi & Ludlow, 2013). During different phases of respiratory cycle there is a precise co-ordination of laryngeal muscles, which is essential for a smoothly airflow to and from the lungs. The laryngeal abductor muscle dilates the glottis during inspiration, decreasing the upper airway resistance to facilitate airflow to the lungs (Brancatisano *et al.* 1991). In contrast, during the early period of expiration, i.e. post-inspiration, the laryngeal adductor muscles slightly narrow the glottis, increasing upper airway resistance to control expiratory airflow (Paton & Dutschmann, 2002). This well co-ordinated control of upper airway resistance maintains a functional residual capacity enough to prevent atelectasis and provides an appropriate period of time for alveolar gas exchange.

The central generation of respiratory-modulated laryngeal movements requires a precise control of laryngeal motoneurones by synaptic inputs from the brainstem respiratory network (Dick *et al.* 1993; Baekey *et al.* 2001). These motoneurones lay within the caudal part of the nucleus ambiguus (NA), the so-called loose formation and retroambiguus nucleus (Irnaten *et al.* 2001; Bautista *et al.* 2012; Hernandez-Morato *et al.* 2013) and several cellular properties and synaptic inputs that may play a role in shaping their firing pattern have been described (Richter *et al.* 1979; Dutschmann & Paton, 2002; Ono *et al.* 2006). However, very little is known about the voltage and time dependence of these cellular properties as well the underlying currents because of the technical limitations involved in studying these features *in vivo* and in identifying the different respiratory-modulated laryngeal motoneurones *in vitro*.

The respiratory control of upper airway resistance is influenced by a wide variety of factors, including hypoxia. Several studies have shown that hypoxia produces a respiratory-related plasticity in the upper airway resistance (Edge *et al.* 2012; Huang *et al.* 2012). It is important to note that the link between hypoxia and changes in the respiratory control of upper airway resistance has a clinical relevance in patients with obstructive sleep apnoea (OSA) (Bradford *et al.* 2005; Mahamed & Mitchell, 2008; Mateika & Narwani, 2009), which experience intermittent upper airway narrowing during natural sleep and hypoxic episodes (Caples *et al.* 2005). Studies performed in humans suggest that acute hypoxia decreases upper airway resistance during breathing (Rowley *et al.* 2007), and that this response is enhanced in patients with OSA (Lee *et al.* 2009). However, there are no studies evaluating the effects of intermittent hypoxia on the respiratory control of upper airway resistance and the electrophysiological mechanisms underlying these changes in the laryngeal motoneurones.

In the present study, we characterized the membrane potential trajectories, intrinsic electrophysiological properties and presence of specific ionic currents in the respiratory-modulated laryngeal motoneurones in the NA of rats. We also investigated the effects of chronic intermittent hypoxia (CIH) on the respiratory control of upper airway resistance and on the intrinsic electrophysiological properties of laryngeal motoneurones. To evaluate the possible role of carotid body (CB) in the generation of changes in the respiratory network and upper airway resistance, a group of rats with CB denervation (CBD) was also submitted to CIH. To reach these goals, we used an anaesthetic-free *in situ* perfused brainstem preparation (Paton, 1996), which allows measurements of upper airway resistance, recordings of nerve activities, as well as whole cell patch clamp recordings of functionally identified laryngeal motoneurones in the intact respiratory network.

Methods

Animals and ethical approval

Experiments were performed on male Wistar rats (100–130 g) obtained from the Animal Care of the University of São Paulo, Campus of Ribeirão Preto, Brazil. The animals were maintained in standard environmental conditions (23 ± 2°C; 12/12 h dark/light cycle) with water and chow *ad libitum*. All experimental protocols were approved by the Ethical Committee on Animal

Experimentation of the School of Medicine of Ribeirão Preto, University of São Paulo (protocols 093/2009 and 064/2010).

Carotid body denervation

Rats were anaesthetized with a ketamine (75 mg kg^{-1} IP)/xylazine (5 mg kg^{-1} IP) mixture. Carotid artery bifurcation was exposed, the carotid sinus nerve and its branches sectioned as previously described (Abdala *et al.* 2012; McBryde *et al.* 2013). To assess the completeness and selectivity of CBD, respiratory and sympathetic responses to activation of peripheral chemoreflex and sympatho-inhibitory response to baroreflex activation were evaluated 2 weeks after CBD in the *in situ* perfused brainstem preparation. Peripheral chemoreceptors were stimulated by injections of potassium cyanide (0.05%, 50 μl) into the descending aorta of the *in situ* preparations. The sympatho-inhibitory response to electrical stimulation of the aortic depressor nerve (ADN; 0.2 ms, three pulses at 400 Hz) was used as an index of barosensitivity (Moraes *et al.* 2012*b*).

Chronic intermittent hypoxia

The CIH, CIH-CBD and control groups of rats were housed in collective cages and maintained in Plexiglas chambers (210 l) equipped with gas injectors and O_2, CO_2, humidity and temperature sensors. The CIH and CIH-CBD (after the 5 day postoperative period) groups were exposed to 5 min of normoxia [fraction of inspired O_2 (F_{I,O_2}) of 20.8%] followed by 4 min of N_2 injection to reduce the F_{I,O_2} to 6%, where it was maintained for periods no longer than 30–40 s. After hypoxia, O_2 was

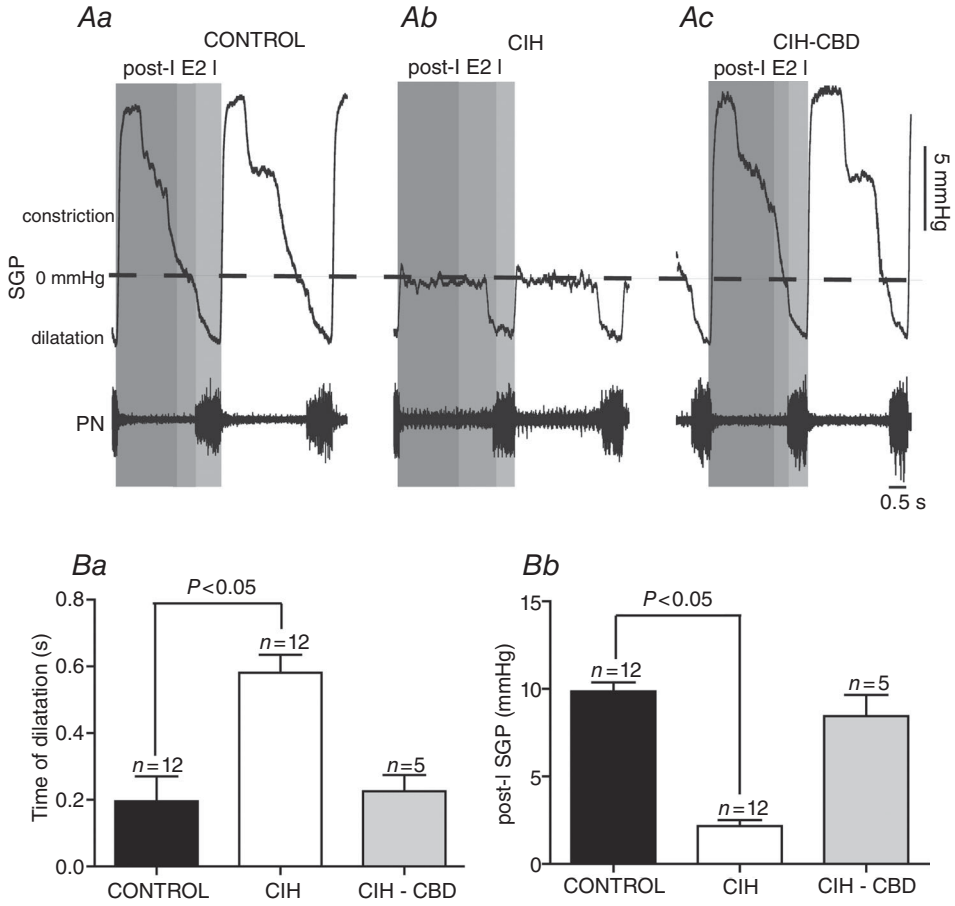

Figure 1. CIH reduces upper airway resistance
A, representative tracings of dynamic changes in glottal resistance during the respiratory cycle, including dilatation during inspiration (decrease in SGP) and constriction in post-I (increase in SGP) from one control (*Aa*), one CIH (*Ab*) and one CIH-CBD (*Ac*), rats. Grouped data comparing the time of glottal dilatation in relation to inspiratory activity (PN; *Ba*) and the magnitude of post-inspiratory glottal constriction (*Bb*) between control, CIH and CIH-CBD rats. Note that CIH exaggerated the inspiratory glottal dilatation, produced a decrease in post-inspiratory glottal constriction and that CBD abolished these changes. CBD, carotid body denervation; CIH, chronic intermittent hypoxia; I, inspiration; post-I, post-inspiration; E2, second half of expiration; PN, phrenic nerve; SGP, subglottal pressure.

injected to return F_{I,O_2} back to 20.8%. This 9 min cycle was repeated 8 h a day (from 09.30 to 17.30 h) for 10 days. The control group was exposed to 20.8% F_{I,O_2}, 24 h a day for 10 days, as described in a previous study from our laboratory (Moraes *et al.* 2013).

Ventral approach of perfused brainstem preparation

Immediately after 10 days of intermittent hypoxia or normoxia, the rats were prepared for *in situ* perfused brainstem preparations. The animals were deeply anaesthetized with halothane (AstraZeneca do Brasil Ltda, Cotia, SP, Brazil), transected caudal to the diaphragm, exsanguinated and submerged in a cooled Ringer's solution (in mM: NaCl, 125; $NaHCO_3$, 24; KCl, 3; $CaCl_2$, 2.5; $MgSO_4$, 1.25; KH_2PO_4, 1.25; dextrose, 10). Rats were then immediately decerebrated at the precollicular level, therefore rendered insentient, and skinned. The ventral medullary surface was exposed for neuronal recording. The preparations were placed supine and all muscles and connective tissues covering the basilar surface of the occipital bone were removed. The basilar portion of occipital bone was removed to expose the ventral surface of the medulla (Moraes *et al.* 2012*b*, 2013). Preparations were then transferred to a recording chamber and the descending aorta was cannulated and perfused with Ringer's solution containing an oncotic agent (1.25% polyethylene glycol; Sigma, St Louis, MO, USA), and continuously gassed with 5% CO_2 and 95% O_2 using a 520S peristaltic pump (Watson-Marlow, Falmouth, UK). For voltage clamp experiments of low voltage activated (LVA) Ca^{2+} currents, the Ringer's solution consisted of (in mM): NaCl, 125; KCl, 3; $MgSO_4$, 1.25; $NaHCO_3$, 24; KH_2PO_4, 1.25; $CaCl_2$, 10; dextrose, 10. The perfusate was warmed to 31°C and filtered using a nylon mesh (pore size: 25 μm; Millipore, Billirica, MA, USA). In preparations, in which we performed neural and neuronal recordings, a neuromuscular blocker was administered (vecuronium bromide, 3–4 μg ml^{-1}; Cristália Produtos Químicos Farmacêuticos Ltda, São Paulo, Brazil).

Electrophysiological data acquisition

Respiratory and sympathetic nerves were isolated and recorded using bipolar glass suction electrodes. Phrenic nerve (PN) activity was recorded from its central end. The superior laryngeal nerve (SLN) was isolated, cut distally and its activity recorded. Abdominal nerve (AbN) was isolated from the abdominal muscles at lumbar level, cut distally and its activity recorded. Recurrent laryngeal nerve (RLN) was isolated for stimulation (see below). The activity of the thoracic sympathetic nerve (tSN)

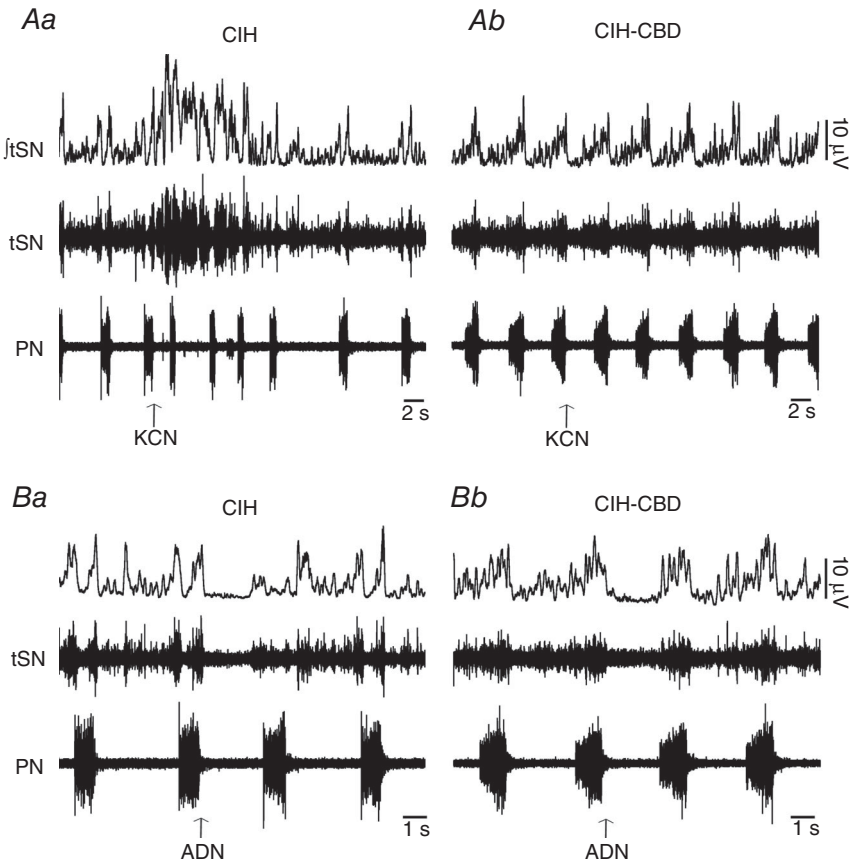

Figure 2. CBD selectively abolished chemoreflex but not baroreflex responses
Raw and integrated (∫) records of tSN and PN activities from one CIH (*Aa*) and one CIH-CBD (*Ab*) rats during baseline and in response to peripheral chemoreflex activation. KCN (0.05%, 50 μl) increased PN and tSN activities in CIH rats, while this response was absent in CIH-CBD rats. Raw and integrated (∫) records of tSN and PN activities from one CIH (*Ba*) and one CIH-CBD (*Bb*) rats during baseline and in response to baroreflex activation. tSN was inhibited in response to ADN (0.2 ms, 3 pulses at 400 Hz) stimulation in both CIH and CIH-CBD rats. ADN, aortic depressor nerve; CBD, carotid body denervation; CIH, chronic intermittent hypoxia; KCN, potassium cyanide; PN, phrenic nerve; tSN, thoracic sympathetic nerve.

was recorded from the sympathetic chain at the level of T8–T12. All signals recorded were amplified, band-pass filtered (0.5–5 kHz) and acquired with an A/D converter (CED 1401; Cambridge Electronic Design, CED, UK), using Spike 2 software (Cambridge Electronic Design).

Blind whole cell patch clamp recordings were performed to study the effects of CIH on membrane potential trajectories, firing frequency, intrinsic electrophysiological properties and to test the presence of outward transient K^+ (I_A), LVA Ca^{2+} and hyperpolarization-activated inward (I_h) currents in inspiratory and post-inspiratory laryngeal motoneurones in the NA. Electrodes were filled with a solution containing (in mM): potassium gluconate, 130; $MgCl_2$, 4.5; trisphosphocreatine, 14; Hepes, 10; EGTA, 5; Na-ATP, 4; Na-GTP, 0.3; biocytin, 0.2%; pH 7.3 and osmolality ~300 mosm/KgH_2O and had resistances of 3–8 MΩ when tested in bath solution. For voltage clamp experiments of LVA Ca^{2+} currents, the electrodes were filled with a solution containing (in mM): $CsCl_2$, 110; TEA, 30; $CaCl_2$, 2; EGTA, 5; $MgCl_2$, 2; Na-ATP, 4; Na-GTP, 0.5; Hepes, 10; biocytin, 0.2%; pH 7.3 and osmolality ~300 mosm/KgH_2O. Electrodes were mounted on a micromanipulator (MHW-3; Narishige, Tokyo, Japan) and positioned onto the ventral surface of the medulla under visual control (microscope; Zeiss, Berlin, Germany) using surface landmarks (trapezoid body, rootlets of the hypoglossal nerve and basilar artery). The caudal NA was mapped by searching for antidromic field potentials following stimulation of the RLN (5–10 V, 1 Hz, 0.2 ms pulse width). Voltage and current clamp experiments were performed using an Axopatch-200B integrating amplifier (Molecular Devices, Sunnyvale, CA, USA) and pClamp acquisition software (version 10.0; Molecular Devices). Gigaseals (>1 GΩ) were formed, and whole cell configuration was obtained by suction.

Ionic currents were measured under voltage clamp with the cell's membrane potential initially held at −70 mV and expressed as pA/pF. Activation properties of I_A were evaluated by applying 10 mV voltage steps (1 s) from −80 to 60 mV, from conditioning steps (500 ms) of either −110 or −40 mV. After off-line subtraction of the currents evoked with holding voltage of −110 and −40 mV, the I_A current was isolated. To maximize I_A and reduce sodium currents, tetrodotoxin (TTX; 0.5 μM; Tocris Bioscience, Bristol, UK) was added to the perfusion solution. LVA Ca^{2+} currents were activated, in the presence of TTX,

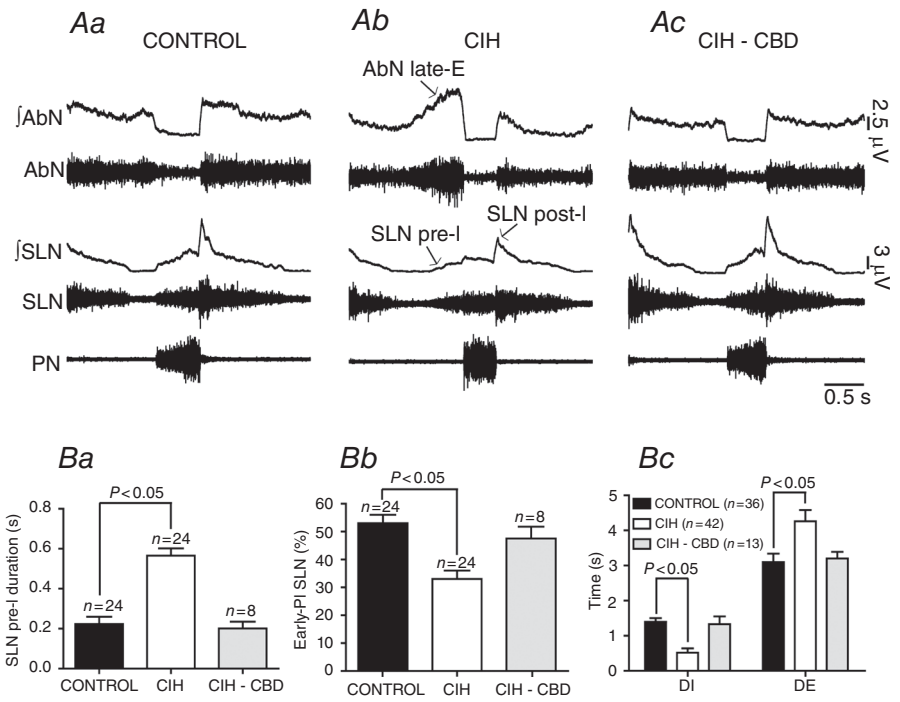

Figure 3. Effects of CIH on the SLN, AbN and PN activities
A, raw and integrated (∫) records of SLN, AbN and PN activities from one control (*Aa*), one CIH (*Ab*) and one CIH-CBD (*Ac*) rats. Note the presence of late-E activity in the AbN, the exaggerated pre-I activity in the SLN in CIH rats and that CBD abolished these changes. Grouped data showing the increase in the SLN pre-I duration (*Ba*), the decrease in the early-PI SLN activity (*Bb*) after CIH and the effects of CBD. *Bc*, CIH also produced a decrease in the DI and an increase in the DE. CBD abolished these changes. AbN, abdominal nerve; CBD, carotid body denervation; CIH, chronic intermittent hypoxia; DE, duration of expiration; DI, duration of inspiration; early-PI, early post-inspiratory; late-E, late-expiratory; PN, phrenic nerve; pre-I, pre-inspiratory; SLN post-I, superior laryngeal nerve post-inspiratory activity.

using a series of depolarizing command pulses (from −90 mV to 40 mV, in 10 mV increments), from a hyperpolarizing conditioning pulse (−90 mV). I_h was activated, in the presence of TTX, using a series of hyperpolarizing voltage pulses (from −60 mV to −140 mV, in 10 mV increments), from a −70 mV conditioning pulse. The ZD7288-sensitive (a selective blocker of I_h current; 40 μM; Sigma-Aldrich, St Louis, MO, USA) component of the hyperpolarizing-evoked currents represents the I_h. The recordings of all ionic currents were also performed in the presence of blockers of fast synaptic transmission in the perfusion solution [2.5–6.0 mM kynurenic acid, 20 μM bicuculline (free-base) and 1 μM strychnine; Sigma-Aldrich] and all signals were low-pass filtered at 1 kHz and sampled at 5 kHz.

In current clamp, all data were low-pass filtered at 5 kHz and digitized at the rate of 20 kHz. The intrinsic electrophysiological properties of laryngeal motoneurones were also evaluated in the presence of blockers of fast synaptic transmission in the perfusion solution.

Measuring subglottal pressure in control, chronic intermittent hypoxia and chronic intermittent hypoxia–carotid body denervation rats

Changes in upper airway resistance were evaluated by direct measurement of subglottal pressure (SGP) (Dutschmann & Paton, 2002). The trachea just below the larynx was cannulated in the direction of the pharynx with a T-shaped catheter. A constant flow of warmed (31°C) and humidified carbogen gas was passed through one arm of this catheter in the expiratory direction. The SGP was recorded via the other side of the T-shaped catheter using a pressure transducer (Model PT 300; Grass, West Warwick, RI, USA). Increases and decreases in the SGP were indicative of constriction (adduction) and dilation (abduction) of the glottis, respectively, thereby giving an index of the dynamic changes in upper airway resistance during the respiratory cycle.

Immunofluorescence

At the end of electrophysiological experiments the preparations were perfused first with phosphate-buffered saline (PBS; 0.1 M) and then with 4% paraformaldehyde and brains removed and post-fixed in 4% paraformaldehyde during 24 h. Transverse sections (30 μm thick) were cut through the NA with a vibrating microtome (Leica, Wetzlar, Germany). The immunofluorescence was performed with free-floating sections. Sections were blocked and permeabilized in PBS containing 10% normal horse serum and 0.5% Triton X-100 for 1 h at room temperature. After three PBS washes, the sections were incubated in primary antibody goat

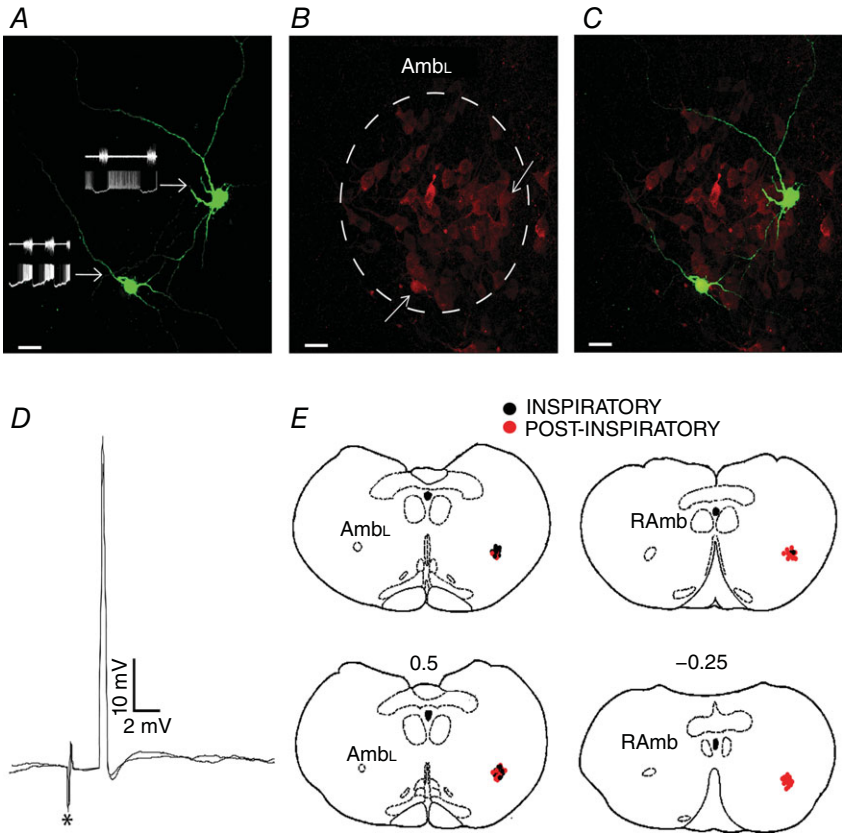

Figure 4. Phenotype of the post-inspiratory and inspiratory laryngeal motoneurones
A, biocytin-labelled post-inspiratory (right side) and inspiratory (left side) laryngeal motoneurones and their representative tracings. *B*, choline acetyltransferase immunohistochemical staining of the AmbL. *C*, merge of (*A*) and (*B*). Note that these laryngeal motoneurones are positive choline acetyltransferase-immunoreactive cells (↑). *D*, representative tracings of two superimposed sweeps of antidromic action potentials in one inspiratory laryngeal motoneurone evoked by stimulation (∗) of the recurrent laryngeal nerve. *E*, sequence of a set of transversal sections corresponding to the levels of caudal part of nucleus ambiguus. Every recorded motoneurone is represented by a colour spot on the same side for better illustration. Numbers on the transversal sections indicate the distance in millimetres to the obex (0). AmbL, loose formation of caudal nucleus ambiguus; RAmb, retroambiguus nucleus.

anticholine acetyltransferase (Chat; 1:500; Millipore) for 24 h at 4°C. After three PBS washes, the sections were incubated in secondary antibodies Alexa 488-conjugated streptavidin (1:1000; Molecular Probes, Grand Island, NY, USA) and Alexa 647-conjugated mouse antigoat (1:500; Molecular Probes) for 1 h at room temperature. Sections were washed three times in PBS and mounted in Fluoromount (Sigma-Aldrich). Images were collected on a Leica TCS SP5 confocal microscope equipped with 488 and 633 nm laser lines and tunable emission wavelength detection.

Data analyses

All analyses of neural recordings were performed off-line in rectified and smoothed (50 ms) signals using Spike 2 software with custom-written scripts. The frequency of PN discharge was determined by the time interval between PN bursts. Active expiration (presence of late-expiratory event in the AbN) was reported when the amplitude of AbN at the end of expiration was greater than the amplitude during post-inspiration. PN-triggered averaging of integrated SLN activity over 20 respiratory cycles was divided into four parts: pre-inspiratory (before PN discharge), inspiratory (coincident with PN discharge), early post-inspiratory (duration of which was defined by the duration of the preceding PN burst) and late post-inspiratory (remaining post-inspiratory activity). The inspiratory and post-inspiratory SLN activities were analysed using areas under the curve in each respiratory part and normalized by the total area, i.e. sum of areas, while the SLN pre-inspiratory activity was analysed using its duration. These analyses were applied for each preparation and the data obtained were pooled together and compared between CIH, CIH-CBD and control groups.

All analyses of neuronal recordings were performed using Clampfit 10 (Molecular Devices), GraphPad 5 and a custom script written in Spike 2 software. The peak conductance for each voltage (G_v) of the I_A was calculated as $G_v = I_{peak}/(V_m - E_K)$, where I_{peak} is peak current, V_m membrane voltage, E_K is the K^+ equilibrium potential calculated from the Nernst equation (Hille, 2001). The relationship between normalized conductance and membrane potential (V_m) was fitted by a Boltzmann function of the form: $G = 1/\{1 + \exp[(V_h - V_m)/V_c]\}$, where G is the relative membrane conductance, V_h is the voltage at half-maximal conductance and V_c is the slope factor. The voltage dependence of I_h activation was obtained from tail currents measured at −80 mV following a series of hyperpolarizing steps; those data were normalized and fitted with an equation of the form: $I/I_{max} = 1/\{1 + \exp[(V_m - V_h)/V_c]\}$. The current–voltage ($I$–$V$) relationship of the LVA Ca^{2+} current was determined from the peak current after the capacitive transient.

Current clamp recordings were analysed off-line to measure: (a) resting membrane potential (RMP); (b) input resistance; (c) amplitude of the afterhyperpolarization potential (AHP); (d) action potential (AP) half-width; (e) numbers of spikes in response to different levels of positive current injection (2 s); and (f) voltage threshold to generate AP. The input resistance was determined via linear regression applied to the linear portion of the I–V relationship. To generate a single AP, a 10 ms depolarizing current pulse of sufficient intensity was applied. AP half-width was measured as the spike width at the half-maximal voltage, while the AHP was measured by subtracting the peak amplitude of the hyperpolarizing deflection after the spike from the threshold for spike initiation. To determine the voltage threshold to generate AP, AP trains were evoked by 1.5 s, 0.4 pA ms^{-1} ramp

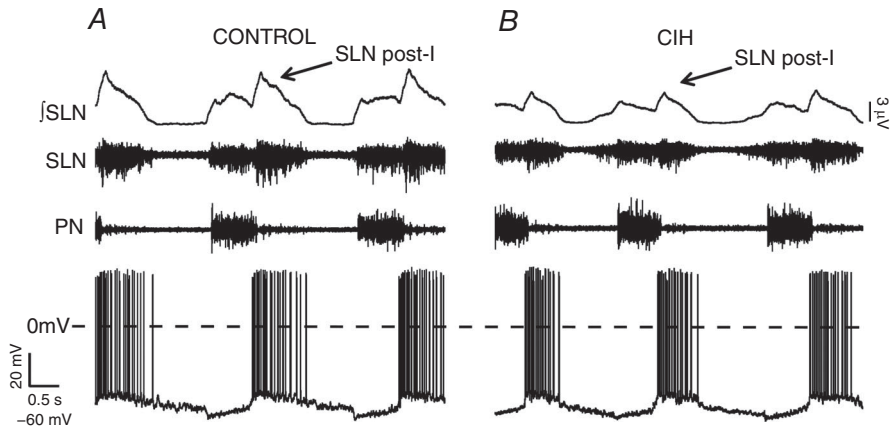

Figure 5. Effects of CIH on post-inspiratory laryngeal motoneurones activities
Raw and integrated (∫) records of SLN, PN and post-inspiratory laryngeal motoneurones activities from one control (*A*) and one CIH (*B*) rats, representatives of their respective groups. Note the pronounced hyperpolarization during the second half of expiration and the decrease in the firing frequency of post-inspiratory laryngeal motoneurone from CIH rat. CIH, chronic intermittent hypoxia; PN, phrenic nerve; post-I, post-inspiratory activity; SLN, superior laryngeal nerve.

current injections and the threshold was determined at the membrane potential once the first AP started to fire.

The index of upper airway resistance was measured from recordings of the SGP (Moraes *et al.* 2014*a*,2014). We measured the peak SGP value of every respiratory cycle during post-inspiration and the time between the pre-inspiratory decrease of the SGP and inspiratory activity (PN) over 30 s periods in control, CIH and CIH-CBD rats. Mean values for these 30 s periods were determined.

Statistical analyses

Results are expressed as mean ± SEM and compared using Student's unpaired *t* test, one-way ANOVA or two-way ANOVA with Bonferroni post-tests, in accordance with the requirements of each experimental protocol. Differences were considered significant when $P < 0.05$.

Results

Dynamics of upper airway resistance in control, chronic intermittent hypoxia and chronic intermittent hypoxia–carotid body denervation rats

Under control conditions, the SGP recordings revealed in all control rats that upper airway resistance decreased before (0.19 ± 0.07 s before the PN discharge; $n = 12$) and during neural inspiration (i.e. coincident with PN discharge), which corresponds to the contraction of abductor muscle (i.e. dilation of the glottis; Fig. 1*Aa*). Glottal constriction occurred immediately after neural inspiration in the post-inspiratory phase as seen by a sharp rise in the SGP (Fig. 1*Aa*). During the second half of expiration (E2 phase), SGP values slowly returned to a steady state, indicating the end of the post-inspiratory phase (Fig. 1*Aa*). In CIH rats, the SGP inspiratory dilatation was exaggerated (0.58 ± 0.05 *vs.* 0.19 ± 0.07 s; $P < 0.05$; Fig. 1*Aa*,*b* and *Ba*) in the E2 phase with no significant changes in the magnitude (2.7 ± 0.9 *vs.* 3 ± 1 mmHg; Fig. 1*Aa*,*b*), while the sharp rise in the SGP during the post-inspiratory phase was significantly reduced (2.1 ± 0.3 *vs.* 9.8 ± 0.5 mmHg; $P < 0.05$; $n = 24$; Fig. 1*Aa*,*b* and *Bb*). These data indicate that the upper airway resistance during post-inspiratory and E2 phases was dramatically reduced in CIH rats.

To evaluate the efficacy of CBD, the PN and tSN responses to potassium cyanide were evaluated in CIH and CIH-CBD rats. Peripheral chemoreflex activation increased PN frequency and tSN activity in CIH rats, while these responses were absents in CIH-CBD rats (Fig. 2*Aa*,*b*). Sympatho-inhibitory response to baroreflex activation was determined by recording the tSN response to ADN stimulation. tSN was inhibited in response to ADN stimulation in both CIH and CIH-CBD rats (Fig. 2*Ba*,*Bb*). These results show that CBD selectively eliminated the peripheral chemoreceptors afferents, but not the afferents of arterial baroreceptors. We next investigated whether the CB neural activity contributes to CIH-induced changes in the respiratory control of upper airway resistance. To test this possibility, we recorded the SGP in CBD rats exposed to CIH. CIH did not alter SGP inspiratory dilatation (0.22 ± 0.04 *vs.* 0.19 ± 0.07 s; Fig. 1*Aa*,*c* and *Ba*) or SGP post-inspiratory constriction (8.4 ± 1.2 *vs.* 9.8 ± 0.5 mmHg; $n = 17$; Fig. 1*Aa*,*c* and *Bb*) in CBD rats in relation to control rats.

Characterization of respiratory pattern in control, chronic intermittent hypoxia and chronic intermittent hypoxia–carotid body denervation rats

To make a possible link between the changes in upper airway resistance recorded from control, CIH and CIH-CBD rats and correspondent changes in the neural control, we performed a study of SLN activity in the different phases of the respiratory cycle. The SLN activity occurred during three phases of respiration. The onset of inspiratory discharge in the PN of control rats was delayed relative to the SLN by 0.22 ± 0.03 s (Fig. 3*Aa*), characterizing a SLN pre-inspiratory activity. The SLN also exhibited

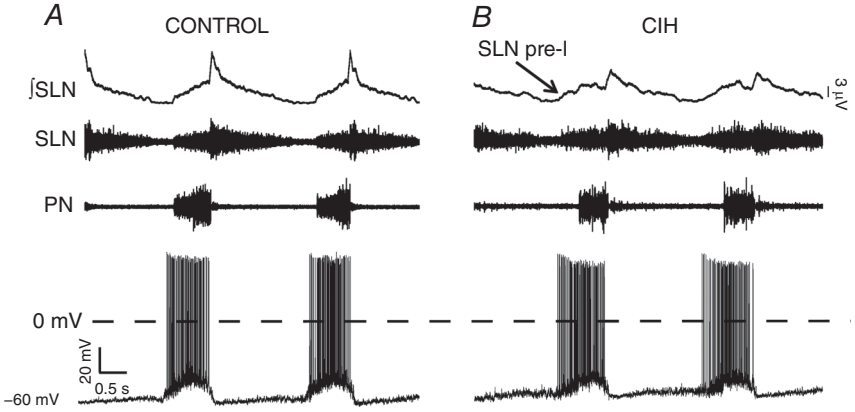

Figure 6. Effects of CIH on inspiratory laryngeal motoneurones activities
Raw and integrated (∫) records of SLN, PN and inspiratory laryngeal motoneurones activities from one control (*A*) and one CIH (*B*) rat, representatives of their respective groups. Note the depolarization during the pre-inspiratory phase, correlated with SLN pre-I activity, increase in firing frequency and depolarization during the post-inspiratory phase of inspiratory laryngeal motoneurone from CIH rat. CIH, chronic intermittent hypoxia; PN, phrenic nerve; pre-I, pre-inspiratory activity; SLN, superior laryngeal nerve.

a burst of central inspiratory activity coincident with PN (Fig. 3*Aa*). Finally, inspiratory discharge was followed by a decrementing post-inspiratory discharge, which was larger in amplitude than the inspiratory discharge (Fig. 3*Aa*). In the CIH group, the SLN pre- and post-inspiratory activities were markedly different in relation to controls. We observed an increase in SLN pre-inspiratory duration (0.56 ± 0.03 *vs.* 0.22 ± 0.03 s; $P < 0.05$; Fig. 3*Aa,b* and *Ba*), in the same phase of AbN active expiration (Fig. 3*Aa,b*), and a decrease in the SLN early post-inspiratory activity (33 ± 3 *vs.* $53 \pm 3\%$; $P < 0.05$; $n = 48$; Fig. 3*Aa,b* and *Bb*) in CIH rats when compared to controls. These data correlate with a decrease in the upper airway resistance during E2 phase/pre-inspiration and post-inspiration after CIH (Fig. 1*Aa,Ab*). CIH also reduced the duration of inspiration–PN (0.52 ± 0.12 *vs.* 1.4 ± 0.1 s; $P < 0.05$) and increased the duration of expiration (4.26 ± 0.32 *vs.* 3.1 ± 0.24 s; $P < 0.05$; Fig. 3*Aa,b* and *Bc*), with no changes in the PN frequency (0.37 ± 0.01 *vs.* 0.35 ± 0.04 Hz; $n = 78$; Fig. 3*Aa,b*).

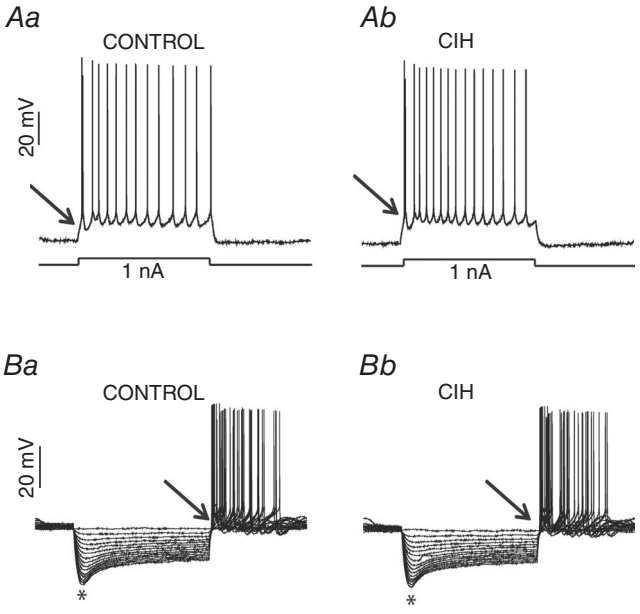

Figure 7. Effects of CIH on the intrinsic electrophysiological properties of post-inspiratory laryngeal motoneurones
In the presence of blockers of fast synaptic transmission (see Methods) in the perfusion, we tested the intrinsic electrophysiological properties of post-inspiratory laryngeal motoneurones from control and CIH rats. Either intrinsic excitability (*Aa* and *Ab*) or input resistance (*Ba* and *Bb*) of post-inspiratory laryngeal motoneurones were not affected by CIH. Note the presence of burst discharge (↑) at the beginning of the positive current injection or at the end of hyperpolarizing pulses in the post-inspiratory laryngeal motoneurones. ∗Upon larger hyperpolarizing pulses in (*Ba*) and (*Bb*) the membrane potential presented a shift toward more positive values as a time-dependent conductance was slowly turned on. CIH, chronic intermittent hypoxia.

We next investigated whether the CB afferents to the neurones of the respiratory network contribute to CIH-induced changes in the respiratory pattern. Similar to the effects of CBD on the CIH-induced changes of upper airway resistance, CIH did not alter the SLN pre-inspiratory duration (0.20 ± 0.03 *vs.* 0.22 ± 0.03 s; Fig. 3*Aa,c* and *Ba*), SLN early post-inspiratory activity (47.5 ± 4.3 *vs.* $53 \pm 3\%$; $n = 32$; Fig. 3*Aa,c* and *Bb*), AbN expiratory activity (Fig. 3*Aa,c*), duration of inspiration (1.33 ± 0.22 *vs.* 1.4 ± 0.1 s) or duration of expiration (3.2 ± 0.19 *vs.* 3.1 ± 0.24 s; $n = 49$; Fig. 3*Aa,c* and *Bc*) in CBD rats.

Membrane potential trajectories and electrophysiological properties of inspiratory and post-inspiratory laryngeal motoneurones from control and chronic intermittent hypoxia rats

Whole cell patch clamp recordings were performed in 60 respiratory-modulated laryngeal motoneurones in the loose formation of NA or in the retroambiguus nucleus (control, $n = 30$; CIH, $n = 30$; Fig. 4*E*). Considering that in CBD rats CIH produced no changes in the upper airway resistance or respiratory pattern, the respiratory-modulated laryngeal motoneurones were not recorded. To be characterized as laryngeal motoneurones the cells should fulfil the following requirements: (a) antidromic excitation from the ipsilateral RLN stimulation with APs occurring at a constant latency (2.2 ± 0.07 ms; $n = 60$; Fig. 4*D*), and (b) the presence of Chat protein (Fig. 4*A–C*). Post-inspiratory motoneurones showed depolarization during post-inspiration and hyperpolarization during E2 and inspiratory phases (Fig. 5*A*), while inspiratory motoneurones showed depolarization during the pre-inspiratory phase, with maximal activity during inspiration, and hyperpolarization during post-inspiration (Fig. 6*A*). Post-inspiratory motoneurones from CIH rats were more hyperpolarized during the E2 phase than post-inspiratory motoneurones from control rats (-59 ± 1 *vs.* -55 ± 1.2 mV; $P < 0.05$; Fig. 5*A* and *B*). CIH also decreased the firing frequency of these motoneurones during post-inspiration (12 ± 1.3 *vs.* 25 ± 1.2 Hz; $P < 0.05$; $n = 12$; Fig. 5*A* and *B*). Regarding inspiratory motoneurones, CIH produced an anticipatory onset of depolarization and generation of APs (0.54 ± 0.02 *vs.* 0.25 ± 0.03 s before the PN activity; $P < 0.05$; Fig. 6*A* and *B*), resulting in increases of firing frequency (79 ± 2 *vs.* 55 ± 3 Hz; $P < 0.05$; Fig. 6*A* and *B*). In addition, CIH produced depolarization of inspiratory motoneurones during post-inspiration (-54 ± 0.9 *vs.* -60 ± 1.1 mV; $P < 0.05$; $n = 12$; Fig. 6*A* and *B*).

To compare the intrinsic electrophysiological properties of post-inspiratory and inspiratory motoneurones and to evaluate whether the effects of CIH on the respiratory

pattern and upper airway resistance, mediated by CB afferents, are dependent on changes in these intrinsic properties, we performed the blockade of their fast synaptic transmission (see Methods). With respect to the CIH effects, no changes were observed in: (a) RMP [(post-inspiratory: -68 ± 2 *vs.* -69 ± 3 mV) (inspiratory: -57 ± 3 *vs.* -59 ± 4 mV)]; (b) number of spikes in response to positive current injection (Figs 7*Aa,b* and 8*Aa,b*); and (c) input resistance ([post-inspiratory: 123 ± 3 *vs.* 121 ± 3 MΩ; $n = 12$; Fig. 7*Ba,b*) (inspiratory: 160 ± 6 *vs.* 152 ± 6 MΩ; $n = 12$; Fig. 8*Ba,b*)]. These findings suggest that the observed CIH-induced decrease in the post-inspiratory and increase in the inspiratory motoneurones activities were due to changes in the respiratory network.

Post-inspiratory and inspiratory laryngeal motoneurones showed similar capacitance (Table 1). However, in relation to the inspiratory, post-inspiratory motoneurones exhibited significantly more negative values of RMP, lower input resistance and excitability, but higher values of AP half-width and AHP (Table 1). In the post-inspiratory motoneurones a burst discharge was evoked (Fig. 7*Ba,b*) at the end of the hyperpolarizing pulses, while in inspiratory motoneurones a delay in the rate of depolarizing was observed (Fig. 8*Ba,b*), suggesting the presence of LVA Ca^{2+} and I_A currents, respectively. In addition, larger negative current injections produced an initial hyperpolarization followed by a shift of the membrane potential toward more positive voltages (sag; Fig. 7*Ba,b*) in the post-inspiratory motoneurones, suggesting the presence of I_h.

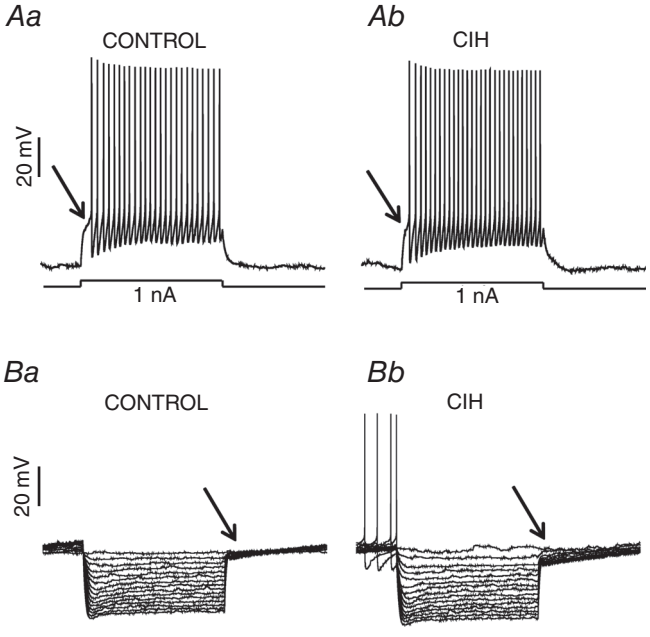

Figure 8. Effects of CIH on the intrinsic electrophysiological properties of inspiratory laryngeal motoneurones
In the presence of blockers of fast synaptic transmission (see Methods) in the perfusion, we tested the intrinsic electrophysiological properties of inspiratory laryngeal motoneurones from control and CIH rats. Either intrinsic excitability (*Aa* and *Ab*) or input resistance (*Ba* and *Bb*) of inspiratory laryngeal motoneurones were not affected by CIH. (↑) Note the delay in the rate of depolarizing at the beginning of the positive current injection or at the end of hyperpolarizing pulses in the inspiratory laryngeal motoneurones. CIH, chronic intermittent hypoxia.

As shown in Fig. 9A, at the end of a hyperpolarizing pulse (constant bias current to −90 mV), a deflection of the voltage trajectory and a low-threshold spike were revealed in the post-inspiratory motoneurone in the presence of TTX. Perfusion of 50 μM Ni^{2+}, a known LVA Ca^{2+} current blocker, but not of ZD7288 (blocker of I_h, 40 μM; Fig. 9*A*), eliminated the low-threshold spike, suggesting that the post-inhibitory rebound in post-inspiratory motoneurones is mediated by LVA Ca^{2+} current. LVA Ca^{2+} currents were activated in post-inspiratory motoneurones from control and CIH rats using a series of depolarizing command pulses (Fig. 9*B*). On average, the peak of activation of LVA Ca^{2+} currents in the post-inspiratory motoneurones was at −40 mV and there was no difference in the LVA Ca^{2+} currents between post-inspiratory motoneurones from control and CIH rats (-4.2 ± 0.19 *vs.* -4.6 ± 0.18 pA/pF; $n = 12$; Fig. 9*C*).

In another experimental protocol, we isolated I_A in inspiratory motoneurones. Depolarizing step commands, from a holding in −110 mV, evoked sustained outward K^+ currents in addition to I_A (Fig. 10*Aa*). We separated I_A from sustained outward K^+ currents by subtraction. Using the same conditions as Fig. 10*Aa*, we applied a sequence of voltage step commands from a holding potential of −40 mV (Fig. 10*Ab*). The difference current was defined as I_A (Fig. 10*Ac*). There is no difference in the average (at 60 mV: 38.8 ± 3.6 *vs.* 40.6 ± 3.2 pA/pF; Fig. 10*B*) or activation properties of I_A between inspiratory motoneurones from control and CIH rats [(half-activation voltage: -33.2 ± 1.9 *vs.* -28.7 ± 1.7 mV) (slope factor: 9.7 ± 1.9 *vs.* 8 ± 1.4 mV; $n = 12$; Fig. 10*C*)].

The post-inspiratory motoneurones also exhibit I_h. Under voltage clamp, hyperpolarizing voltage steps (−60 to −140 mV), from a holding potential of −70 mV, revealed a slowly activating inward current (Fig. 11*Aa*). Addition of ZD7288 (40 μM) to the perfusion resulted in a significant reduction in this current (Fig. 11*Ab*). Off-line subtraction of the inward current before and after perfusion with ZD7288 revealed the I_h, which starts to be activated about −80 mV. There is no difference in the average (at −140 mV: -9.3 ± 0.6 *vs.* -8.5 ± 0.7 pA/pF $n = 12$; Fig. 11*B*) or activation properties of I_h between post-inspiratory motoneurones from control and CIH rats [(half-activation voltage: -106.8 ± 1.4 *vs.* -110.7 ± 1.3 mV) (slope factor: -11.7 ± 1.7 *vs.* -11.3 ± 1.4 mV; $n = 12$; Fig. 11*C*)]. The sag observed in the post-inspiratory motoneurones

Table 1. Electrophysiological properties of respiratory laryngeal motoneurones

Neuronal types	*n*	Cm (pF)	RMP (mV)	R_i (MΩ)	Excitability (mV)§	AHP (mv)	AP half-width (ms)
Inspiratory	6	115 ± 15	−57 ± 3	160 ± 6	−35 ± 1.9	3 ± 0.7	0.6 ± 0.07
Post-inspiratory	6	108 ± 12	−68 ± 2†	123 ± 3*	−30 ± 0.9‡	7 ± 0.4*	1.1 ± 0.05*

Mean values of the electrophysiological properties of post-inspiratory and inspiratory laryngeal motoneurones recorded from control rats. Abbreviations: AHP, afterhyperpolarization potential; AP, action potential; Cm, capacitance; R_i, input resistance; RMP, resting membrane potential. *$P < 0.001$; †$P = 0.01$; ‡$P < 0.05$; §membrane potential threshold to generate AP.

in response to larger hyperpolarizing pulses was also eliminated by perfusion of ZD7288 (Fig. 11*D*).

Discussion

In this study, we used integrative and cellular approaches to investigate the effects of CIH on the neural respiratory control of upper airway resistance. Using an *in situ* preparation, we showed that CIH produces a significant reduction in the upper airway resistance of rats, by changes in the SLN pre- and post-inspiratory activities, which seems to be an important adaptation for the temporal co-ordination of cranial and spinal motor outputs in response to intermittent hypoxic episodes. Importantly, selective denervation of the CB abolished CIH-induced changes in the respiratory pattern and consequently in the upper airway resistance. The present study also describes the electrophysiological properties of respiratory laryngeal motoneurones and the effects of CIH. The data show that CIH increased the inspiratory and decreased the post-inspiratory laryngeal motoneurone activities, independent of any changes in their intrinsic electrophysiological properties. Therefore, all changes in the upper airway resistance in response to CIH seem to be determined by the CB-induced changes in the central generator for breathing that drives laryngeal motoneurones. These neural changes in the respiratory network seem to be an adaptive process required for an appropriated pulmonary ventilation and control of upper airway resistance under intermittent episodes of hypoxia.

We observed that CIH produced a significant increase in the SLN pre-inspiratory activity. This finding is consistent with our kinesiological experiments of respiratory control of upper airway resistance showing that CIH exaggerated pre-inspiratory glottal abduction, thereby increasing time for pulmonary gas exchange. On the other hand, post-inspiratory glottal constriction is essential to prevent lungs collapse and atelectasis (Bartlett, 1986). In this regard, CIH decreased post-inspiratory SLN activity and glottal adduction, which would severely compromise attempts at exhalation and consequently will disrupt the breathing pattern (Harding, 1984). The present study also demonstrates that the CIH effects on respiratory motor activity, as shown before for the development of sympathetic overactivity (Peng *et al.*

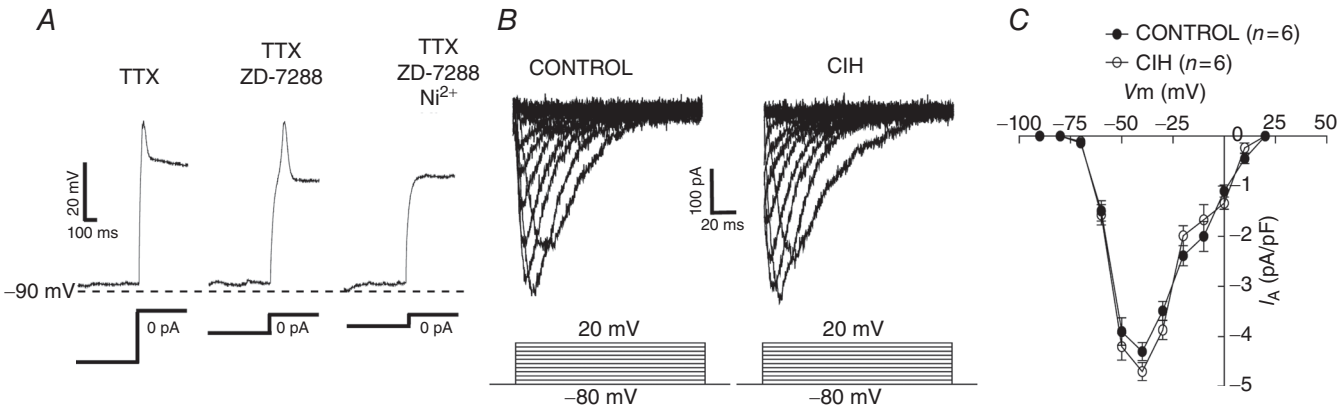

Figure 9. LTS and low voltage activated Ca^{2+} currents in the post-inspiratory laryngeal motoneurones
A, examples of electrophysiological recordings obtained from one representative post-inspiratory laryngeal motoneurone from control rats showing the generation of LTS at the end of a hyperpolarizing pulse as a short-lasting depolarizing hump in the presence of TTX (0.5 μM). The LTS was entirely blocked by addition of 50 μM Ni^{2+}, but not by ZD7288 (40 μM), a selective blocker of the I_h, to the perfusion solution. *B*, low voltage activated Ca^{2+} currents in the post-inspiratory laryngeal motoneurones from control and CIH rats in response to a series of depolarizing command pulses, from a hyperpolarizing conditioning pulse of −90 mV. *C*, average peak amplitudes of the evoked currents as a function of the command potential in the post-inspiratory laryngeal motoneurones from control and CIH rats. CIH, chronic intermittent hypoxia; LTS, low-threshold spike; TTX, tetrodotoxin.

2014) and hypertension (Fletcher *et al.* 1992), are entirely dependent on CB afferents. As the baroreflex function was preserved in CBD rats, the absence of CIH-induced changes in the respiratory pattern and upper airway resistance can be related to the lack of neural inputs from the CB. The mechanisms underlying the CB chemoreflex-induced changes in the respiratory network after CIH remain elusive. Several studies suggest that oxidative stress is the major cellular mechanism underlying the CIH-induced autonomic changes (Prabhakar *et al.* 2007; Yuan *et al.* 2011). Evidence includes that CIH-induced oxidative stress and hypoxia-inducible factor 1-mediated upregulation of pro-oxidant enzymes in the ventral medulla are dependent on CB neural activity (Peng *et al.* 2014). However, it remains to be investigated whether similar changes occur in respiratory neurones involved in the generation of respiratory rhythm and pattern in this subregion of the ventral medulla.

Whole cell patch clamp recordings were made from Chat-positive motoneurones in caudal NA, which axons are in the RLN and they probably drive laryngeal muscles. Accordingly, two classes of respiratory laryngeal motoneurones can be found within the caudal NA (Barillot *et al.* 1990; Bryant *et al.* 1993): inspiratory and post-inspiratory. We speculate that synaptic inputs from pre-Bötzinger Complex (pre-BötC)/rostral ventral respiratory group pre-inspiratory neurones contribute to shaping the inspiratory-related changes in the inspiratory motoneurone membrane potential of control and CIH rats, which activity is consistent with inspiratory motoneurones recorded *in vivo* anaesthetized rats (Bautista *et al.* 2010). On the other hand, the membrane potential trajectories of inspiratory motoneurones during expiration suggest the existence of some inhibition during post-inspiration. This possibility is supported by results of experiments using chloride iontophoresis in inspiratory laryngeal motoneurones (Takeda & Haji, 1988; Barillot *et al.* 1990). However, the source of these inhibitory inputs has not yet been identified. BötC post-inspiratory neurones, due to their firing patterns, are candidates for this inhibitory source (Smith *et al.* 2007), and it may derive from direct synaptic inputs of neurones located in the Kölliker–Fuse nucleus of dorsolateral pons (Dutschmann & Herbert, 2006). Considering that CIH produced an anticipatory onset of depolarization and generation of APs during pre-inspiration and decreased the post-inspiratory hyperpolarization of inspiratory motoneurones, independent of any intrinsic electrophysiological properties, additional experiments will be required to identify precisely the CB-induced changes in the membrane trajectory potential as well as in the intrinsic electrophysiological properties of medullary inspiratory and post-inspiratory neurones driving changes in the

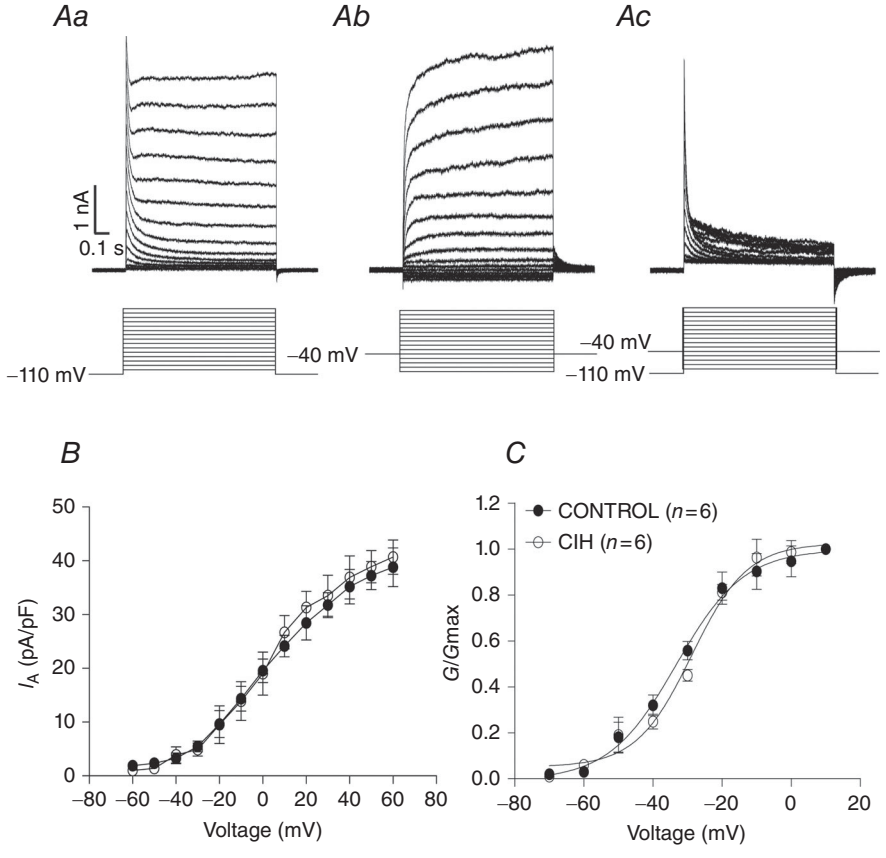

Figure 10. Outward transient K^+ currents (I_A) in the inspiratory laryngeal motoneurones
Aa, voltage clamp recording from a holding potential of −110 mV illustrating the I_A evoked at depolarized membrane potentials in the inspiratory laryngeal motoneurone representative of the control rats. Ab, voltage clamp recording from a holding potential of −40 mV illustrating the lack of significant I_A evoked at depolarized membrane potentials. Ac, I_A was isolated by subtracting the current traces in (*Aa*) from (Ab), while the voltage clamp protocols are shown superimposed. *B*, mean amplitude of peak component of I_A in the laryngeal inspiratory motoneurones from control and CIH rats. *C*, average normalized I_A amplitude in the laryngeal inspiratory motoneurones from control and CIH rats obtained with the voltage-dependent activation protocol plotted as a function of the command potential (Boltzman fitted; see Methods). CIH, chronic intermittent hypoxia.

inspiratory motoneurones after CIH. We suggest that the late-E neurones of the retrotrapezoid nucleus/parafacial respiratory group, which are activated in conditions of active expiration (Abdala *et al.* 2009; Pagliardini *et al.* 2011; Moraes *et al.* 2012*a*), may be the source of increased synaptic inputs to inspiratory motoneurones during pre-inspiration in CIH rats. This possibility may explain the generation of coupled active expiration and exaggerated upper airway dilatation in CIH rats.

Studying the membrane potential trajectories of post-inspiratory motoneurones from control rats, we observed excitation during post-inspiration, as described previously in cats (Richter *et al.* 1979; Takeda & Haji, 1988; Barillot *et al.* 1990), and inhibition during inspiration and E2 phase. Dutschmann and Paton (2002) demonstrated that during glycine receptor antagonism, post-inspiratory motoneurones depolarized and shifted their phase of firing to inspiration. We also observed that post-inspiratory motoneurones from CIH rats present a pronounced hyperpolarization during the E2 phase, which seems to be important to avoid any increase in the upper airway resistance before inspiration. Taking into account these findings, we suggest that post-inspiratory motoneurones from control and CIH rats receive glycinergic inhibition, probably from pre-BötC early inspiratory neurones (Smith *et al.* 2013), and CIH increased the synaptic inhibition during the E2 phase. The source of this increase in the E2 phase synaptic inhibition is also a matter for further experiments, but we suggest that BötC augmenting-expiratory inhibitory neurones are candidates for this inhibitory source (Fortuna *et al.* 2008; Smith *et al.* 2013), rising from their firing patterns in conditions of active expiration (Moraes *et al.* 2014*a*).

With respect to post-inspiratory excitation of the post-inspiratory motoneurones, several studies in cats and rats (Gauthier *et al.* 1983; Sun *et al.* 2008) suggested that post-inspiratory activity depends on post-inhibitory rebound rather than excitatory inputs. However, the blockade of inspiratory inhibition did not eliminate post-inspiratory depolarization in post-inspiratory motoneurones of rats (Dutschmann & Paton, 2002). On the other hand, we observed depolarization, and bursts of APs, mediated by LVA Ca^{2+}

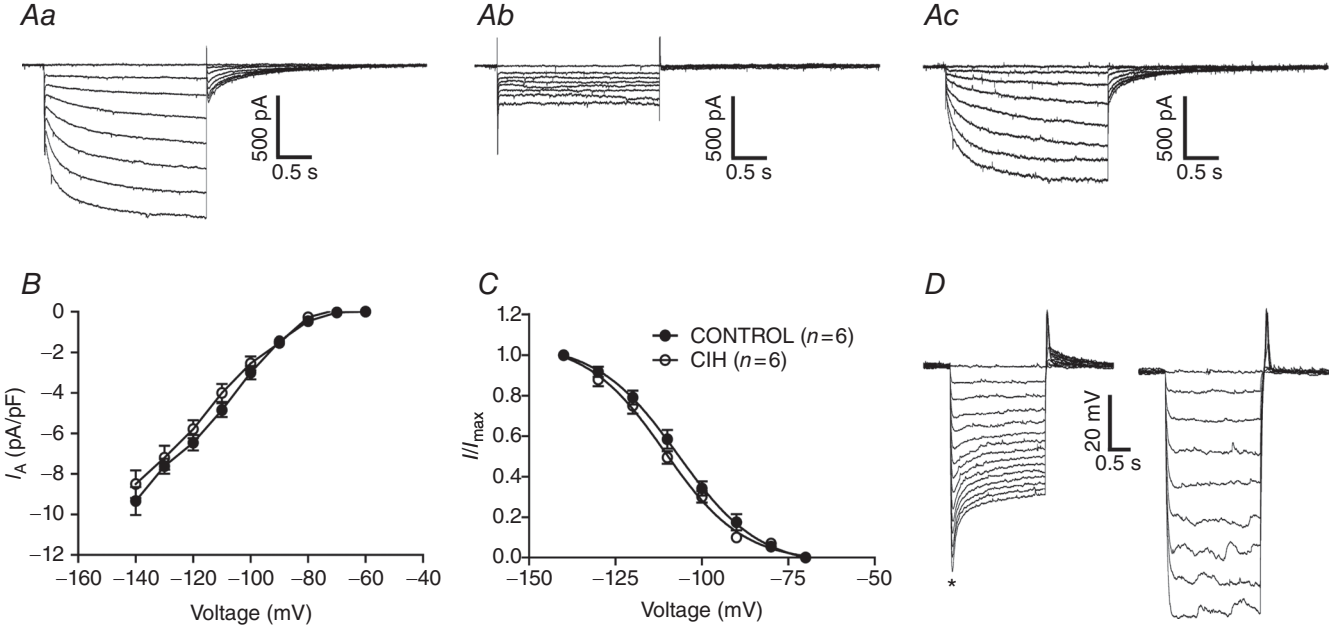

Figure 11. Hyperpolarization-activated inward currents (I_h) in the post-inspiratory laryngeal motoneurones
Aa, voltage clamp recording of one representative post-inspiratory laryngeal motoneurone from control rats showing that hyperpolarizing voltage steps (−10 mV increments), from a holding potential of −70 mV, evoked a time-dependent inward current. *Ab*, inward current is reduced by addition of ZD7288 (40 μM), a selective blocker of the I_h, to the perfusion solution. *Ac*, off-line subtraction of the traces presented in (*Aa*) and (*Ab*) is showing the ZD7288-sensitive I_h. *B*, current–voltage relationship of the steady-state portion of the averaged I_h in the post-inspiratory laryngeal motoneurones from control and CIH rats. *C*, I_h activation curve (Boltzman fitted; see Methods) showing its voltage dependence. *D*, voltage transients of one post-inspiratory laryngeal motoneurone representative of control rats in response to hyperpolarizing current injections. Upon larger hyperpolarizing pulses, the membrane potential relaxed towards more positive values as a time-dependent conductance slowly turned on (*sag; left panel). Addition of ZD7288 to the perfusion blocked the hyperpolarization-activated conductance and eliminated the sag (right panel). CIH, chronic intermittent hypoxia.

current, when the post-inspiratory motoneurones were released from hyperpolarization after synaptic blockade. These findings support the concept that the expiratory depolarization of post-inspiratory motoneurones, and consequent post-inspiratory glottal constriction, are due to the combination of excitatory synaptic inputs and Ca^{2+}-mediated post-inhibitory rebound. Considering that CIH decreased the firing frequency of post-inspiratory motoneurones, with no changes in their intrinsic electrophysiological properties or in the LVA Ca^{2+} currents, additional experiments will be important to evaluate the effects of CIH, mediated by CB afferents, on other medullary post-inspiratory neurones.

The intrinsic electrophysiological properties of post-inspiratory and inspiratory motoneurones were also compared. Post-inspiratory motoneurones exhibited more negative RMP, lower excitability and input resistance when compared with inspiratory motoneurones, indicating that post-inspiratory motoneurones are less excitable. The lower excitability of post-inspiratory motoneurones is consistent with their adaptive firing pattern during post-inspiration; and the higher excitability of inspiratory motoneurones is consistent with their phasic inspiratory bursting pattern. The large AHP and AP half-width may also underlie the decrementing firing frequency of post-inspiratory motoneurones in the intact respiratory network. The presence of I_h in post-inspiratory motoneurones indicates that it will affect how these motoneurones integrate the respiratory synaptic inputs. The I_h may prevent prolonged or excessive hyperpolarization in response to inhibitory synaptic inputs without compromising depolarizing responses to excitatory inputs in the post-inspiratory motoneurones. On the other hand, inspiratory motoneurones showed the presence of delay excitation mediated by I_A, which was confirmed by voltage clamp experiments. This current may contribute to shape the ramp pattern of inspiratory motoneurones as described in medullary pre-inspiratory neurones (Hayes *et al.* 2008).

An important question in the context of the effects of CIH on the respiratory pattern is related to the functional implication of the observed changes in upper airway resistance. In patients with OSA, anatomical vulnerability of the upper airway facilitates the occurrence of obstructions during sleep (White, 2006), but these patients try to adapt to this challenging condition generating a higher level of activity in their upper airway dilating muscles (Mezzanotte *et al.* 1992). Our findings using CIH, an important component of OSA, indicate that changes in upper airway resistance in response to hypoxia are dependent on the CB-induced changes in the respiratory central pattern generator. These changes represent a novel mechanism by which upper airway motor tone adapts to the conditions imposed by intermittent hypoxia. In our understanding, the exaggerated pre-inspiratory dilatation of the upper airway may serve to enhance the stability of breathing during and following hypoxic stimulus to preserve an appropriate gas exchange. In addition, SLN pre-inspiratory activity increased in parallel with the AbN late expiratory event in CIH rats, reducing the upper airway resistance during active expiration. On the other hand, the decreased post-inspiratory SLN activity and glottal constriction after CIH reduces upper airway stability, demonstrating the detrimental effects of CIH on the respiratory control of upper airway resistance. The data of the present study show important changes in upper airway resistance and laryngeal motoneurone activities after CIH, which are dependent on the CB-induced changes in the central respiratory generators. These findings contribute to a better understanding of the mechanisms underlying the upper airway resistance adjustments in response to intermittent hypoxia.

References

Abdala AP, McBryde FD, Marina N, Hendy EB, Engelman ZJ, Fudim M, Sobotka PA, Gourine AV & Paton JF (2012). Hypertension is critically dependent on the carotid body input in the spontaneously hypertensive rat. *J Physiol* **590**, 4269–4277.

Abdala AP, Rybak IA, Smith JC & Paton JF (2009). Abdominal expiratory activity in the rat brainstem-spinal cord *in situ*: patterns, origins and implications for respiratory rhythm generation. *J Physiol* **587**, 3539–3559.

Baekey DM, Morris KF, Gestreau C, Li Z, Lindsey BG & Shannon R (2001). Medullary respiratory neurones and control of laryngeal motoneurones during fictive eupnoea and cough in the cat. *J Physiol* **534**, 565–581.

Barillot JC, Grelot L, Reddad S & Bianchi AL (1990). Discharge patterns of laryngeal motoneurones in the cat: an intracellular study. *Brain Res* **509**, 99–106.

Bartlett DJ (1986). The respiratory system, upper airway motor systems. In *Handbook of Physiology*, ed. Cherniack NS, pp. 223–245. American Physiological Society, Bethesda, MD.

Bautista TG, Sun QJ & Pilowsky PM (2012). Expiratory-modulated laryngeal motoneurons exhibit a hyperpolarization preceding depolarization during superior laryngeal nerve stimulation in the *in vivo* adult rat. *Brain Res* **1445**, 52–61.

Bautista TG, Sun QJ, Zhao WJ & Pilowsky PM (2010). Cholinergic inputs to laryngeal motoneurons functionally identified in vivo in rat: a combined electrophysiological and microscopic study. *J Comp Neurol* **518**, 4903–4916.

Bradford A, McGuire M & O'Halloran KD (2005). Does episodic hypoxia affect upper airway dilator muscle function? Implications for the pathophysiology of obstructive sleep apnoea. *Respir Physiol Neurobiol* **147**, 223–234.

Brancatisano A, Dodd DS & Engel LA (1991). Posterior cricoarytenoid activity and glottic size during hyperpnea in humans. *J Appl Physiol* **71**, 977–982.

Bryant TH, Yoshida S, de Castro D & Lipski J (1993). Expiratory neurons of the Botzinger Complex in the rat: a morphological study following intracellular labeling with biocytin. *J Comp Neurol* **335**, 267–282.

Caples SM, Gami AS & Somers VK (2005). Obstructive sleep apnea. *Ann Intern Med* **142**, 187–197.

Dick TE, Oku Y, Romaniuk JR & Cherniack NS (1993). Interaction between central pattern generators for breathing and swallowing in the cat. *J Physiol* **465**, 715–730.

Dutschmann M & Herbert H (2006). The Kolliker-Fuse nucleus gates the postinspiratory phase of the respiratory cycle to control inspiratory off-switch and upper airway resistance in rat. *Eur J Neurosci* **24**, 1071–1084.

Dutschmann M & Paton JF (2002). Glycinergic inhibition is essential for co-ordinating cranial and spinal respiratory motor outputs in the neonatal rat. *J Physiol* **543**, 643–653.

Edge D, Bradford A, Jones JF & O'Halloran KD (2012). Chronic intermittent hypoxia alters genioglossus motor unit discharge patterns in the anaesthetized rat. *Adv Exp Med Biol* **758**, 295–300.

Fletcher EC, Lesske J, Behm R, Miller CC 3rd, Stauss H & Unger T (1992). Carotid chemoreceptors, systemic blood pressure, and chronic episodic hypoxia mimicking sleep apnea. *J Appl Physiol (1985)* **72**, 1978–1984.

Fortuna MG, West GH, Stornetta RL & Guyenet PG (2008). Botzinger expiratory-augmenting neurons and the parafacial respiratory group. *J Neurosci* **28**, 2506–2515.

Fregosi RF & Ludlow CL (2013). Activation of upper airway muscles during breathing and swallowing. *J Appl Physiol (1985)* **116**, 291–301.

Gauthier P, Hilaire G & Monteau R (1983). Onset and control of expiratory laryngeal discharge: cross-correlation analysis. *Respir Physiol* **54**, 67–77.

Harding R (1984). Perinatal development of laryngeal function. *J Dev Physiol* **6**, 249–258.

Hayes JA, Mendenhall JL, Brush BR & Del Negro CA (2008). 4-Aminopyridine-sensitive outward currents in preBotzinger complex neurons influence respiratory rhythm generation in neonatal mice. *J Physiol* **586**, 1921–1936.

Hernandez-Morato I, Pascual-Font A, Ramirez C, Matarranz-Echeverria J, McHanwell S, Vazquez T, Sanudo JR & Valderrama-Canales FJ (2013). Somatotopy of the neurons innervating the cricothyroid, posterior cricoarytenoid, and thyroarytenoid muscles of the rat's larynx. *Anat Rec (Hoboken)* **296**, 470–479.

Hille B (2001). *Ionic Channels of Excitable Membranes*, 3rd edn. Sinauer Associates, Sunderland, MA.

Huang H, Zhang X, Ding N, Li Q & Min Y (2012). Effects of chronic intermittent hypoxia on genioglossus in rats. *Sleep Breath* **16**, 505–510.

Irnaten M, Wang J & Mendelowitz D (2001). Firing properties of identified superior laryngeal neurons in the nucleus ambiguus in the rat. *Neurosci Lett* **303**, 1–4.

Lee DS, Badr MS & Mateika JH (2009). Progressive augmentation and ventilatory long-term facilitation are enhanced in sleep apnoea patients and are mitigated by antioxidant administration. *J Physiol* **587**, 5451–5467.

Mahamed S & Mitchell GS (2008). Simulated apnoeas induce serotonin-dependent respiratory long-term facilitation in rats. *J Physiol* **586**, 2171–2181.

Mateika JH & Narwani G (2009). Intermittent hypoxia and respiratory plasticity in humans and other animals: does exposure to intermittent hypoxia promote or mitigate sleep apnoea? *Exp Physiol* **94**, 279–296.

McBryde FD, Abdala AP, Hendy EB, Pijacka W, Marvar P, Moraes DJ, Sobotka PA & Paton JF (2013). The carotid body as a putative therapeutic target for the treatment of neurogenic hypertension. *Nat Commun* **4**, 2395.

Mezzanotte WS, Tangel DJ & White DP (1992). Waking genioglossal electromyogram in sleep apnea patients versus normal controls (a neuromuscular compensatory mechanism). *J Clin Invest* **89**, 1571–1579.

Moraes DJ, Bonagamba LG, Costa KM, Costa-Silva JH, Zoccal DB & Machado BH (2014*a*). Short-term sustained hypoxia induces changes in the coupling of sympathetic and respiratory activities in rats. *J Physiol* **52**, 2013–2033.

Moraes DJ, da Silva MP, Bonagamba LG, Mecawi AS, Zoccal DB, Antunes-Rodrigues J, Varanda WA & Machado BH (2013). Electrophysiological properties of rostral ventrolateral medulla presympathetic neurons modulated by the respiratory network in rats. *J Neurosci* **33**, 19223–19237.

Moraes DJ, Dias MB, Cavalcanti-Kwiatkoski R, Machado BH & Zoccal DB (2012*a*). Contribution of the retrotrapezoid nucleus/parafacial respiratory region to the expiratory-sympathetic coupling in response to peripheral chemoreflex in rats. *J Neurophysiol* **108**, 882–890.

Moraes DJ, Machado BH & Paton JF (2014*b*). Specific respiratory neuron types have increased excitability that drive presympathetic neurones in neurogenic hypertension. *Hypertension* **63**, 1309–1318.

Moraes DJ, Zoccal DB & Machado BH (2012*b*). Sympathoexcitation during chemoreflex active expiration is mediated by L-glutamate in the RVLM/Botzinger complex of rats. *J Neurophysiol* **108**, 610–623.

Ono K, Shiba K, Nakazawa K & Shimoyama I (2006). Synaptic origin of the respiratory-modulated activity of laryngeal motoneurons. *Neuroscience* **140**, 1079–1088.

Pagliardini S, Janczewski WA, Tan W, Dickson CT, Deisseroth K & Feldman JL (2011). Active expiration induced by excitation of ventral medulla in adult anesthetized rats. *J Neurosci* **31**, 2895–2905.

Paton JF (1996). A working heart-brainstem preparation of the mouse. *J Neurosci Methods* **65**, 63–68.

Paton JF & Dutschmann M (2002). Central control of upper airway resistance regulating respiratory airflow in mammals. *J Anat* **201**, 319–323.

Peng YJ, Yuan G, Khan S, Nanduri J, Makarenko VV, Reddy VD, Vasavda C, Kumar GK, Semenza GL & Prabhakar NR (2014). Regulation of hypoxia-inducible factor-α isoforms and redox state by carotid body neural activity in rats. *J Physiol* **592**, 3841–3858.

Prabhakar NR, Kumar GK, Nanduri J & Semenza GL (2007). ROS signaling in systemic and cellular responses to chronic intermittent hypoxia. *Antioxid Redox Signal* **9**, 1397–1403.

Richter DW, Camerer H, Meesmann M & Rohrig N (1979). Studies on the synaptic interconnection between bulbar respiratory neurones of cats. *Pflügers Arch* **380**, 245–257.

Rowley JA, Deebajah I, Parikh S, Najar A, Saha R & Badr MS (2007). The influence of episodic hypoxia on upper airway collapsibility in subjects with obstructive sleep apnea. *J Appl Physiol* **103**, 911–916.

Shiba K, Nakazawa K, Ono K & Umezaki T (2007). Multifunctional laryngeal premotor neurons: their activities during breathing, coughing, sneezing, and swallowing. *J Neurosci* **27**, 5156–5162.

Smith JC, Abdala AP, Borgmann A, Rybak IA & Paton JF (2013). Brainstem respiratory networks: building blocks and microcircuits. *Trends Neurosci* **36**, 152–162.

Smith JC, Abdala AP, Koizumi H, Rybak IA & Paton JF (2007). Spatial and functional architecture of the mammalian brain stem respiratory network: a hierarchy of three oscillatory mechanisms. *J Neurophysiol* **98**, 3370–3387.

Sun QJ, Berkowitz RG & Pilowsky PM (2008). GABA A mediated inhibition and post-inspiratory pattern of laryngeal constrictor motoneurons in rat. *Respir Physiol Neurobiol* **162**, 41–47.

Takeda R & Haji A (1988). Electrophysiological properties of respiratory laryngeal motoneurons and effects of thiopental. *Tohoku J Exp Med* **156**(Suppl), 21–31.

White DP (2006). The pathogenesis of obstructive sleep apnea: advances in the past 100 years. *Am J Respir Cell Mol Biol* **34**, 1–6.

Yuan G, Khan SA, Luo W, Nanduri J, Semenza GL & Prabhakar NR (2011). Hypoxia-inducible factor 1 mediates increased expression of NADPH oxidase-2 in response to intermittent hypoxia. *J Cell Physiol* **226**, 2925–2933.

Additional information

Competing interests

None declared.

Author contributions

D.J.A.M. was responsible for the conception, design of experiments, collection, analysis, data interpretation and writing the manuscript. B.H.M. was involved in the conception, data interpretation and writing the manuscript. All authors have read and approved the final submission.

Funding

This work was supported by grants from 'Fundação de Amparo à Pesquisa do Estado de São Paulo' (FAPESP, Thematic Project to BHM, 2009/50113-0, 2013/06077-5, Research Grant to DJAM, 2013/10484-5 and a post-doctoral fellowship to DJAM, 2011/24050-1).